Kufa Journal of Engineering
Vol. 17, No. 3, July 2026, P.P. 719-731
Article history: Received 16 December 2025, last revised 13 January 2026, accepted 21 January 2026

EXPERIMENTAL AND CFD INVESTIGATION OF THE THERMAL PERFORMANCE OF GRAPHITE-COATED ALUMINUM PLATE HEAT SINKS

Nabeel Abdulhadi Ghyadh

Department of Mechanical Engineering, Faculty of Engineering, Kufa University, 54002, Najaf, Iraq, Emailnabeel.ghayadh@uokufa.edu.iq.

https://doi.org/10.30572/2018/KJE/170341

ABSTRACT

Because next-generation electronic devices are compact and have high power densities, efficient cooling techniques are required to improve a heat sink's thermal performance and keep the temperature at a safe level. A graphite layer was applied to the aluminium substrate. Two aluminum specimens were prepared for testing; one has a graphite covering, while the other specimen is left uncoated for comparison. A wind tunnel was developed to study the heat transfer coefficient to comprehend the performance of the Al heat sink coated with graphite. To replicate the energy produced by a heat sink, a plate electrical heater is affixed to the specimen's bottom. The distribution of body temperature, thermal transmittance, and Nusselt number with four Reynolds number values under turbulent flow conditions for each sample was examined experimentally and numerically using a three-dimensional CFD-solid-mechanics model. The findings demonstrated that graphite enhances thermal performance. An improvement of approximately almost 15.2% in Nusselt number and 38% in thermal transmittance was observed compared to the uncoated case, with the graphite-coated sample exhibiting the most effective thermal dissipation and the uncoated sample exhibiting the worst.

KEYWORDS

Graphite coating, Aluminum plate heat sink, Thermal performance, Forced convection, CFD simulation.

1. INTRODUCTION

Many large power and heat exchange systems have general issues with thermal management and heat dispersion. At least in the electronics systems, high heat generation has been noted. Since 1965, the semiconductor industry, which forms the core of the electronics sector, has adhered to Moore's law (Manno et al., 2015). Understanding and optimizing heat transfer mechanisms are essential for designing efficient systems and devices. The three primary forms of heat transfer are radiation, convection, and conduction. Although each model has importance, convection is especially noteworthy because of its broad applicability and influence on real-world situations (Murtadha et al., 2024). The most challenging aspect, nowadays, facing researchers is the thermal aspect of application workloads, electronic devices such as those used in smartphones, which are associated with a large number of integrated circuits and operate for many hours, while the small size of such devices is demanded. The dissipation of the generated heat in such devices is an important factor in increasing their abilities, especially in hardware. For this reason, many researchers have focused on managing the generated heat in electronic components. It is mainly done by improving the surface of the heat sink, either by increasing the surface area or by coating the surface of the heat sink with materials that increase heat emission, such as graphite and graphene (Al-Baghdadi, 2020; Shahil and Balandin, 2012).

Lately, numerous forms of heat exchanger edifices have been designed with the intend to enhance the ratio of heat transfer, and at the same time to minimize the least distance feasible (Kareem et al., 2025). Graphite materials are increasingly favored over conventional thermal management options such as aluminum and copper due to their combination of low weight and superior heat conduction capability. In the field of electronics, cooling, thin graphite foils represent the most widely adopted form. Unlike metals, these sheets display strong anisotropic behavior, meaning characteristics such as thermal conductivity, electrical resistance, and thermal expansion differ markedly between the in-plane and through-thickness directions (Cermak et al., 2017).

Several studies have been proposed to deal with the enhancement of heat dissipation. According to Sarvar et al. (Sarvar et al., 2006), every metal surface is rough because of tiny hills, valleys, and poor surface topography or texture. A layer of interstitial air separates the surface from the electronic parts. Heat transfer is greatly reduced by the low thermal conductivity of the air that fills these gaps. In light of the aforementioned, scientists have undertaken a number of theoretical and practical investigations aimed at improving heat transmission. Investigated by (Premkumar et al.,2024), the experiments measuring temperature fluctuations of heat sinks with lateral fins coated with graphene and carbon nanotubes (CNTs) under heat inputs of 15–45 W showed that coatings significantly influence heat dissipation and time to reach target temperatures (40–60 °C). Graphene coatings enhanced heat transfer by up to 1.15, while CNT coatings achieved a 1.9 enhancement at lower heat input (15 W). The infrared spectroscopy confirmed retention of energy on the fins, heat sinks and convective cooling fins on the central rows. It has been established that operating temperature, input energy, type of nanocoating, and thickness of the nanocoating are influential parameters that affect the performance of heat sinks. Mixed-material coatings are promising for the enhancement of heat dissipation. (Hadi et al., 2021) conducted experimental research on the impact of graphite and graphene coatings applied on hot surfaces and the influence on heat dissipation performance. For experimental evaluation, three aluminum alloys were prepared, and these were the uncoated sample that served as the reference, the sample coated with graphite, and the sample coated with graphene. To decrease the thermal contact resistance, a single heat sink with good thermal conductivity was sandwiched between the heater plate and the base plate of the heat sink. These experiments were conducted for four values of the Reynolds number (turbulent flow). The results of the experiments indicate that the highest capacity for heat dissipation was exhibited by the sample coated with graphene, while the sample with no coating exhibited thermal performance that was considered to be the least adequate. Wei-Yu and associates (Tsai et al.) evaluated the application of aluminum alloys as heat sinks in conjunction with LED lighting; the thermal dissipation efficiency of the radiation was enhanced by application of High Emissive coatings on the Al substrate. In order to enhance thermal dissipation, different ceramic combinations, including Al2O3, SiO2, and graphite, were inserted using the ultrasonic mechanical coating with armoring (UMCA) technology. Analytical heat flow formulations have been employed to couple radiation and convection at the surface of test samples, with theoretical results showing strong agreement with experimental findings. Incorporating ceramic powders into aluminum heat sinks has been shown to decrease surface temperature by approximately 5–11 °C, offering advantages for cooling-related applications. Through parametric studies, (Jones and Smith, 1970) identified the optimum fin spacing that maximizes heat dissipation from a defined reference plane using the mean heat transfer coefficient across multiple horizontal arrays. (Ning Li et al., 2025) In space applications, spacecraft heat dissipation primarily relies on thermal radiation. To reduce weight, aluminum radiators are preferred over copper, but their lower emissivity limits thermal performance. Recent work has shown that incorporating modified reduced graphene oxide (mRGO) into an epoxy coating can enhance aluminum emissivity and heat dissipation. Using Joule heating to reduce graphene oxide followed by surface modification, a graphene/epoxy composite coating (GERC) was prepared, achieving high emissivity (up to 0.93) and optimal heat dissipation efficiency (24.15%) with 4 wt% mRGO. The coating also demonstrated excellent adhesion and thermal stability, offering a promising approach for space radiator thermal management. In another study focused on natural convection (Icoz and Arik, 2010) assessed lightweight carbon-based structures—including graphite foils—based on their thermal performance index, determining carbon foam to be the most efficient candidate. They also reported that the relatively low cross-plane conductivity of graphite sheets did not hinder overall fin performance. Supporting this observation, (Sabatino and Yoder (2014) performed numerical simulations of pyrolytic graphite applied in finned heat sinks and flat-plate thermal spreaders for circuit board cooling, which confirmed these outcomes.

The primary objective of this study is to enhance heat dissipation from aluminum surfaces through the application of graphene coatings. To ensure safety and prevent any hazards to human health, the graphene layers are applied using a controlled, automated chemical spray technique. This research combines both CFD modeling and experimental investigation, providing a comprehensive understanding of thermal performance. Unlike previous studies, the experiments are conducted on samples of actual practical size, rather than idealized or miniature models, allowing for results that are more applicable to real-world applications. Furthermore, the study systematically examines the effect of graphene coating on heat transfer under varying Reynolds numbers, both numerically using COMSOL Multiphysics and empirically in a forced convection wind tunnel with a range of air velocities. This dual approach enables a thorough assessment of the coating's impact on thermal performance, bridging the gap between theoretical predictions and practical implementation.

2. METHODOLOGY

2.1. Experimental setup

To supply airflow into the experimental setup, a centrifugal blower with adjustable speed was attached to one end of a rectangular channel measuring 2300 mm in length and constructed from thermally insulated polycarbonate glass Fig. 1. The duct cross-section measured 100 × 100 mm with a hydraulic diameter of 100 mm. The test section was positioned 1800 mm (12Dh) downstream of the air inlet to ensure that the flow was fully developed before reaching the measurement zone. Fig. 2 illustrates a photograph and surface morphology of uncoated and graphite-coated aluminium plate heat sinks**.** A plate heater, designed with the same size as the base plate, was employed to deliver uniform heat flux to the bottom surface of the heat sink. Power to the heater was supplied by a programmable DC unit, enabling precise control of the input energy. To minimize contact resistance between the heater and the heat sink base, a high-conductivity thermal interface compound (HC-131) was applied.

Temperature monitoring was achieved using five Fluke 87 thermocouples (USA), which recorded values at the heat sink base, the duct wall surfaces, the air inlet and outlet of the test section, and the surrounding environment. The mean inlet velocity inside the duct was obtained using anemometers positioned downstream of the flow straightener. To analyze the thermal distribution across the upper surface of the compact heat sinks, a high-resolution infrared thermal camera (FLIR E50, USA) was utilized. Additionally, the mean surface temperature of the heat sink was measured with an infrared thermometer. For thermographic evaluation, the top wall of the duct above the test region was removed, allowing infrared imaging of the heat sink surface. Steady-state conditions were assumed after approximately 30 minutes, as the temperature variation remained within ±0.1 °C.

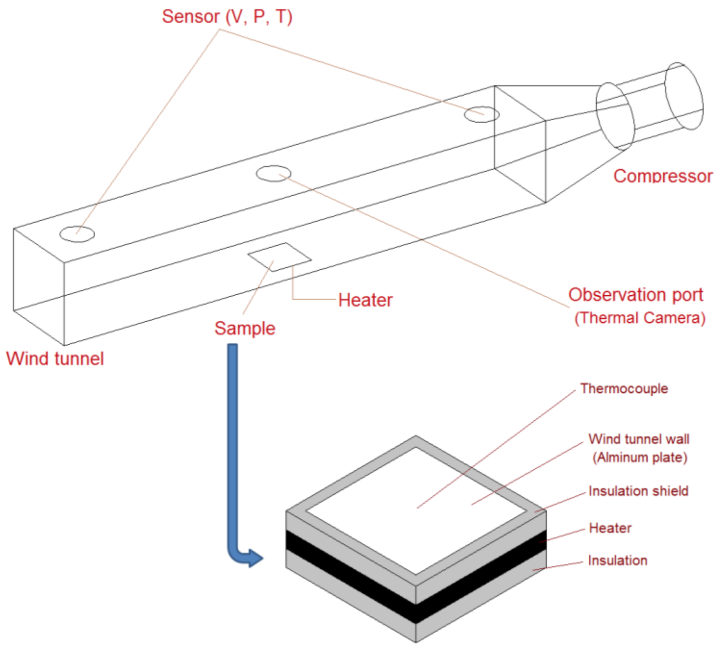

(a)

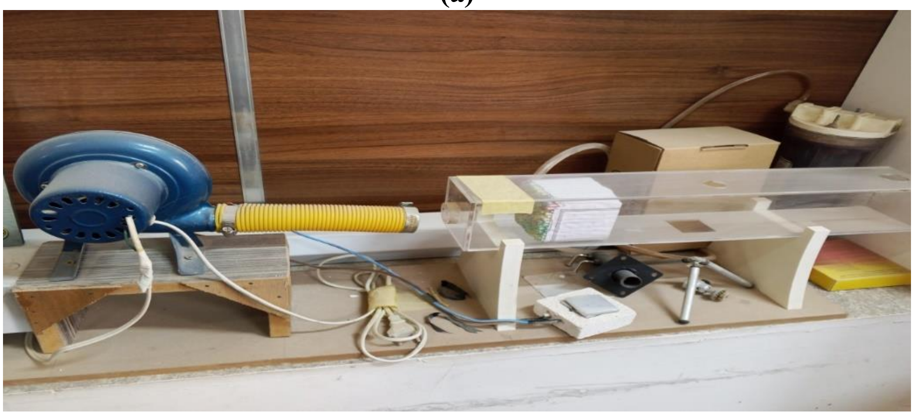

(b)

Fig. 1.a: A schematic diagram showing the location and configuration of the instrumentation in the wind tunnel. b- real photographic image for the test rig.

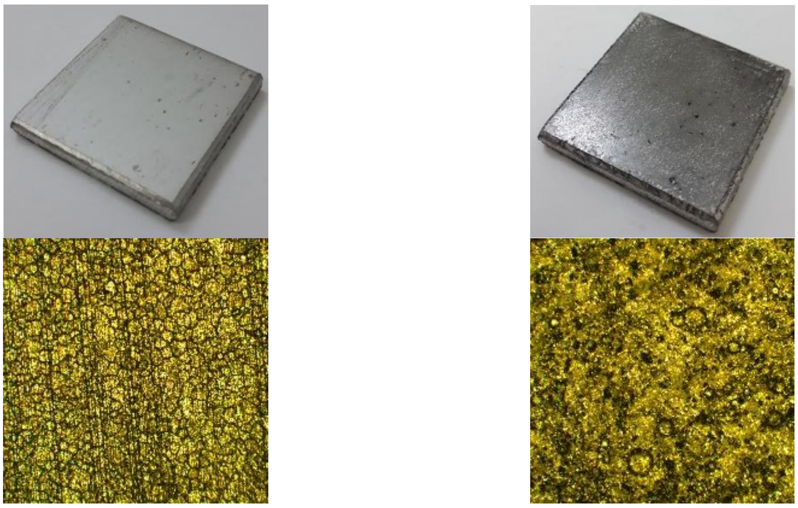

Aluminum **Graphite coated**

Fig. 2. A photograph and surface morphology of uncoated and graphite-coated aluminium plate heat sinks.

The following features of heat transfer and fluid air flow are present in a wind tunnel equipped with a heat sink, where heat is first transferred from the heater to the heat sink by conduction. Convection and radiation occur only from the heat sink surfaces to the surrounding air and wind tunnel walls. Convective heat transfer Q_c transfers the majority of the power q_{power} that the heater provides into the air flow to the heat sink sample, while radiative heat transfer q_{ra} transfers a small but significant power portion q_{power} into the wind channel walls. radiative and Convective heat fluxes are denoted by q_{ra} and Q_c , respectively.

The following equations express the convection heat transfer;

$$Q_c = q_{power} - q_{ra} - Q_k \tag{1}$$

The equation of conductive heat transfer.

$$Q_k = k\left(T_s - T_g\right) \tag{2}$$

In this relation, k denotes the thermal conductivity of the specimen, while Tg corresponds to the temperature recorded by the thermocouple positioned on the sample's surface.

Below is the equation of radiative heat transfer;

$$q_{ra} = \sigma\epsilon A(T_s^4 - T_w^4) \tag{3}$$

Here, σ represents the Stefan–Boltzmann constant, A is the exposed surface area of the specimen, ε is the emissivity of the surface (Maher, 2020), Tw is the temperature of the wind tunnel wall, and Ts is the specimen temperature obtained from a thermocouple embedded at its center.

$$Q_c = q_{power} - \sigma\epsilon A(T_s^4 - T_w^4) - k\left(T_s - T_g\right) \tag{4}$$

The following equation calculates the power provided by the heater;

$$Q_{power} = V.I = \frac{V^2}{R} \tag{5}$$

The following equation calculates the thermal transmittance T_r (Hadi, et al.,2021):

$$T_r = \frac{Q_c}{(T_s - T_a)} \tag{6}$$

Since, T_a is the air temperature.

$$T_r = \frac{Q_{power} - \sigma.\epsilon.A.(T_s^4 - T_w^4) - k.(T_s - T_g)}{(T_s - T_a)} \tag{7}$$

The equations following express convective heat transfer.

$$h = \frac{Q_c}{A.(T_s - T_a)} \tag{8}$$

$$h = \frac{Q_{power} - \sigma.\epsilon.A.(T_s^4 - T_w^4) - k.(T_s - T_g)}{A.(T_s - T_a)} \tag{9}$$

The Reynolds number is;

$$Re_L = \frac{u.L}{\nu} \tag{10}$$

where L is the sample characteristic heated edge, u is the mean air velocity inside the wind tunnel, ν is the air kinematic viscosity.

The Nusselt number is given by;

$$Nu = \frac{h.L}{k} \tag{11}$$

and Prandtl number can be calculated by;

$$Pr = \frac{\nu}{\alpha} \tag{12}$$

In this equation, α denotes the thermal diffusivity of air.

2.2. Experimental uncertainties

The max. Nusselt and Reynolds numbers uncertainties have been calculated using Moffat's method (Moffat, R.J., 1985). According to this experiment work, the parameters' uncertainty (i.e., Re, T, and Nu) has been estimated as follows:

eT = ±√ (e12 + e٢2 + e٣2 + …) (13)

In this equation, ei represents the measurement uncertainty. According to these calculations, Re and Nu have maximum uncertainties of 2.6% and 4.4%, respectively.

2.3. Experimental validation

To verify the accuracy of the present measurements, the Nusselt number obtained for the bare plate was benchmarked against previously reported experimental studies. Fig. 3 illustrates the comparison over a range of Reynolds numbers between the current results and those published by (Sara, 2003; Bilen et al.,20011; Bhatti and Shah, 1987), and (Sahin and Demir, 2008). The outcome of this comparison confirms that the experimental setup used in this work is consistent with established findings in the literature.

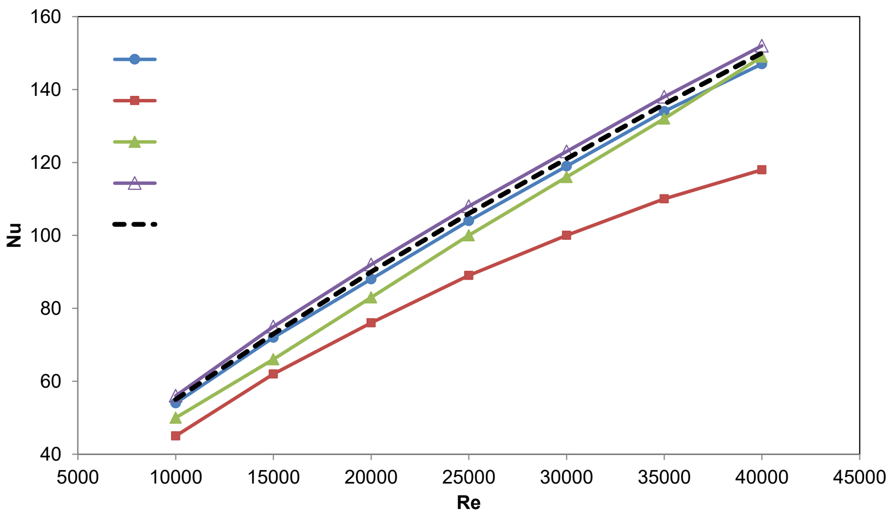

Fig. 3. Different experimental results are compared by Nusselt numbers for standard plate heat sink (Δ: (Sara, 2003; Bilen et al.,2001), (Bhatti and Shah, 1987), and (Sahin and Demir, 2008), — —: the experimental data of work)

2.4. Numerical simulation model

Reynolds Average Navier-Stokes (RANS) equations govern the flow field entirely in three dimensions. The following momentum and continuity equations are used for a Newtonian incompressible fluid;

$$\rho\nabla.\mathrm{U} = 0 \tag{14}$$

$$\rho\left(\frac{\partial \mathrm{U}}{\partial t} + \mathrm{U}.\nabla\mathrm{U}\right) = -\nabla\mathrm{P} + \nabla.\left[\mu(\nabla\mathrm{U} + (\nabla\mathrm{U})^{\mathrm{T}})\right] - \nabla.\overline{(\rho u' \otimes u')} + \mathrm{F} \tag{15}$$

where ⊗: is the outer vector product, and U: is the average velocity.

The following equations uses Turbulence k-ω model:

$$\frac{\partial \rho k}{\partial t} + \nabla.(\rho u k) = P_k - \rho\beta^* k\omega + \nabla.\left((\mu + \sigma^*\mu_T)\nabla k\right) \tag{16}$$

$$\rho\frac{\partial \omega}{\partial t} + \rho u\,.\nabla\omega = \alpha\frac{\omega}{k}P_k - \rho\beta\omega^2 + \nabla.\left((\mu + \sigma\mu_T)\nabla\omega\right) \tag{17}$$

where

$$\mu_T = \rho\frac{k}{\omega} \tag{18}$$

$$\alpha = \frac{13}{25} \qquad \beta = \beta_o f_\beta \qquad \beta^* = \beta_o^* f_\beta \qquad \sigma = \frac{1}{2} \qquad \sigma^* = \frac{1}{2} \tag{19}$$

$$\beta_o = \frac{13}{125} \qquad f_\beta = \frac{1 + 70X_\omega}{1 + 80X_\omega} \qquad X_\omega = \left|\frac{\Omega_{ij}\ \ \Omega_{jk}\ \ S_{ki}}{(\beta_o^*\omega)^3}\right| \tag{20}$$

$$\beta_o^* = \frac{9}{100} f_\beta^* = \begin{cases} 1 & X_k \leq 0 \\ \dfrac{1 + 680X_k^2}{1 + 400X_k^2} & X_k > 0 \end{cases} \qquad X_k = \frac{1}{\omega^3}(\nabla k\,.\nabla\omega) \tag{21}$$

where ω_{ij} is the mean tensor of rotation rate.

$$\Omega_{ij} = \frac{1}{2}\left(\frac{\partial u_i}{\partial x_j} - \frac{\partial u_j}{\partial x_i}\right) \tag{22}$$

S_{ij} represents the tensor mean strain rate.

$$S_{ij} = \frac{1}{2}\left(\frac{\overline{\partial u_\iota}}{\partial x_j} - \frac{\overline{\partial u_J}}{\partial x_i}\right) \tag{23}$$

$$P_k = 2\mu_T\left(\mathrm{S}:\mathrm{S} - \frac{1}{3}(\nabla.\mathbf{u})^2\right) - \frac{2}{3}\rho k(\nabla.\mathbf{u}) \tag{24}$$

Where $\mathrm{S} = \frac{1}{2}(\nabla\mathbf{u} + (\nabla\mathbf{u})^T)$, μ_f, p, ρ_f, and u are the dynamic viscosity [N.s/m2], pressure [Pa], density [kg/m3], and velocity [m/s] respectively for the fluid.

Energy balance equation

$$u.\nabla T = \frac{k_f}{\rho_f.Cp}\nabla^2 T \tag{25}$$

In this equation, k_f represents the thermal conductivity of the fluid [W/m·K], Cp is its specific heat capacity [J/kg·K], ρ_f is the fluid density, and T denotes the temperature [K].

The solid region energy equation is

$$k_s.\nabla^2 T = 0 \tag{26}$$

In this expression, the subscript s refers to the solid, while f denotes the fluid.k_s represents the thermal conductivity of the solid material [W/m·K].

Since the thin layer of graphite is thinner than the typical lengths of the overall model, the thin layer of solid materials can be considered a boundary. Solving the following equation for heat transfer at solid-solid interfaces:

$$d_s\rho C_p\frac{\partial T}{\partial t} + \nabla_t.\mathbf{q} = d_sQ + q_o \tag{27}$$

$$\mathbf{q} = -d_s.k_{graphite}.\nabla_t T \tag{28}$$

d_s refers to the graphite thickness layer [m], the Q refers to the heat source density distributed in the graphite layer, while the heat flux received out of plane is noted by q_o.

A constant heat flux was applied to the base of the heat sink. The simulation assumed a no-slip condition at solid surfaces, ambient pressure at the outlet, an inlet air temperature of 25 °C, and uniform inlet velocity. The outer walls of the rectangular flow channel were considered thermally insulated. Numerical simulations were carried out using COMSOL Multiphysics. To ensure grid independence, detailed tests were performed by comparing the average heat sink temperatures and Nusselt numbers across different mesh sizes (Raad H. et al., 2023). Convergence was achieved when the relative difference between successive iterations in all variables fell below 1.0×10−6.

3. RESULTS AND DISCUSSION

Comparison of the experimental and numerical approaches. A thermographic camera experiment was conducted in order to compare the results with a CFD model used to estimate the heat sink surface temperature Fig. 4. Obviously, the CFD simulation results and the thermal imaging camera results are extraordinarily similar, as seen from the heat spots in the simulation results. Overall, the results are very consistent in terms of their consistency. Using simulation analysis to predict the temperature field of coated material heat sinks, these results confirm that the temperature field of coated material heat sinks can be accurately predicted.

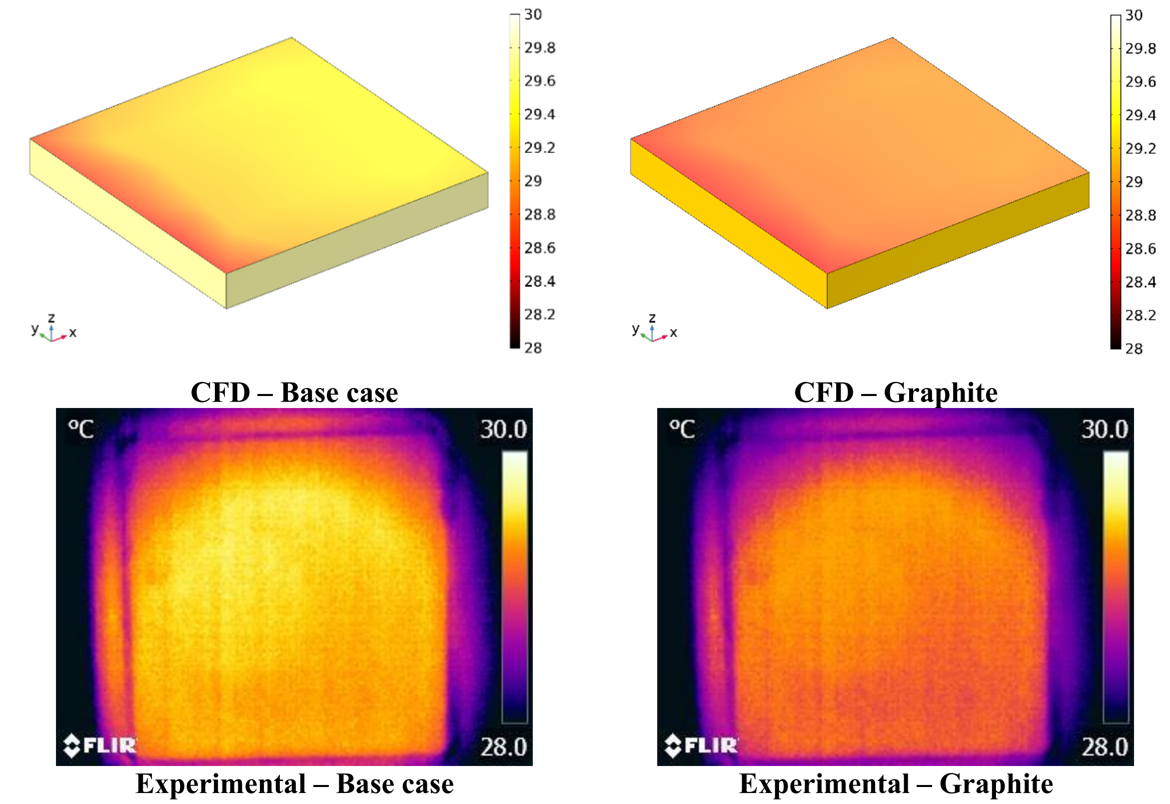

Fig. 4. Comparison of the temperature distribution for the coated and uncoated heat sink plate using the thermal image and CFD simulation results, Re=3000.

The earlier portion of this section reported the heat transfer characteristics for the coated surface as opposed to the non-coated surface derived from the current investigation.

In relation to the graphite coating, the different heat transfer performance characteristics were investigated both experimentally and numerically. For a range of Reynolds numbers, numerical results and experiments are obtained.

For Reynolds numbers of 3000, 5000, 7000, 9000, and 11000, the thermal transmittance, Nusselt numbers, and heat transfer coefficients over tested coated and uncoated heat sinks are displayed numerically in Figs. 5 and 6.

The Nusselt number (Nu) and thermal transmittance (Tr) were evaluated for turbulent airflow over a range of Reynolds numbers to quantitatively assess the performance of both coated (graphite) and uncoated heat sinks. The figure presents the measured Nusselt numbers, heat transfer characteristics, and thermal transmittance values for each heat sink across Reynolds numbers from 3000 to 11,000. The results indicate that the coated heat sinks exhibit higher Nu and thermal transmittance, which is attributed to the graphene layer's superior thermal conductivity and its roughened, island-like surface that increases the effective heat transfer area. An improvement of approximately almost 15.2% in Nusselt number and 38% in thermal transmittance was observed compared to the uncoated case.

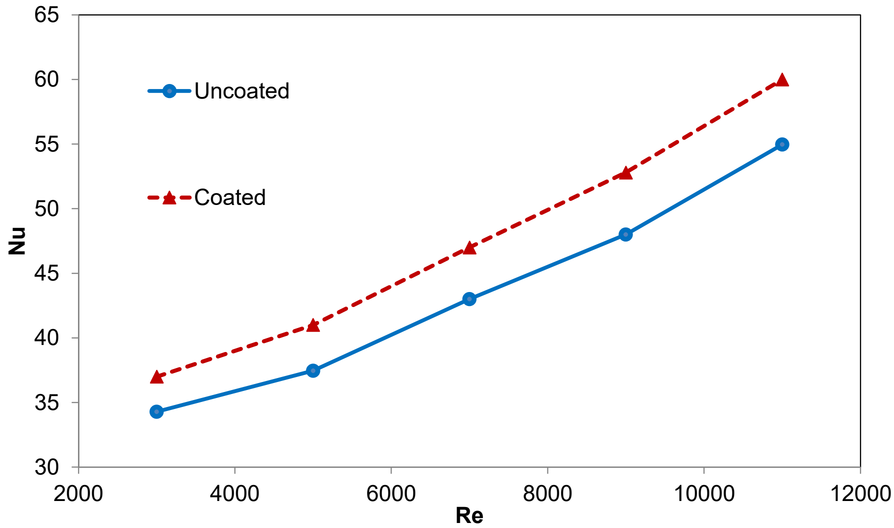

Fig. 5. Nusselt numbers for uncoated and graphite-coated aluminum plate heat sinks.

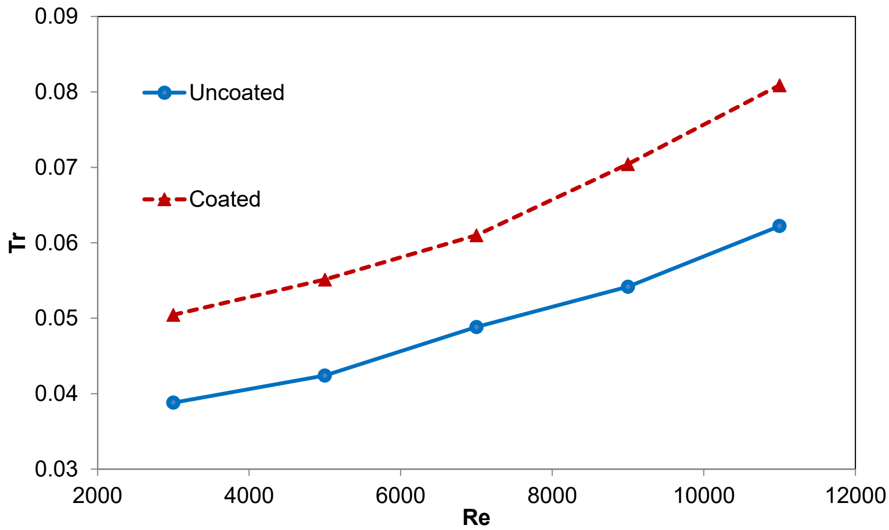

Fig. 6. Thermal transmittance for uncoated and graphite-coated aluminum plate heat sinks.

4. CONCLUSIONS

Two samples of aluminum heat sinks are studied numerically in the COMSOL program and experimentally tested in a wind tunnel. One of them has been coated with graphite, while the other specimen is pure aluminum for the judging task. The experiments and numerical simulations were conducted in turbulent Reynolds number. From the calculation of Nusselt number and the thermal transmittance, it is concluded that: The coating process provides best heat transfer enhancement with graphite nanoparticles results. An improvement of approximately almost 15.2% in Nusselt number and 38% in thermal transmittance were observed compared to uncoated case. The enhancements of the thermal transmittance at all *Re* numbers . And Using simulation analysis to predict the temperature field of coated material heat sinks, these results confirm that the temperature field of coated material heat sinks can be accurately predicted.

5. REFERENCES

Al-Baghdadi, M.A.S. (2020) Graphene Coating for Efficient Electronics Cooling. MDPI, Encyclopedia, Switzerland, pp.1-12.

Bhatti, M.S. (1987) Turbulent and transition flow convective heat transfer in ducts. Handbook of single-phase convective heat transfer.

Bilen, K., Akyol, U. and Yapici, S. (2001) 'Heat transfer and friction correlations and thermal performance analysis for a finned surface', Energy Conversion and Management, 42(9), 1071-1083.

Cermak, M., Kenna, J., and Bahrami, M., 2017, March. Natural-graphite-sheet based heat sinks. In 2017, 33rd Thermal Measurement, Modeling & Management Symposium (SEMI-THERM) (pp. 310-313) IEEE.

Hadi, A.M., Ismael, M.A. and Alhattab, H.A. (2021) 'Improvement of heat sink performance using graphite and graphene coating', Basrah J. Eng. Sci, 21(1), 50-55.

Icoz, T. and Arik, M. (2009) 'Light weight high performance thermal management with advanced heat sinks and extended surfaces', IEEE Transactions on Components and Packaging Technologies, 33(1), 161-166.

Jones, C.D. and Smith, L.F. (1970) 'Optimum arrangement of rectangular fins on horizontal surfaces for free-convection heat transfer', Journal of Heat Transfer, 92(1), 6-10.

Kareem J. Alwan, Radhwan A. Flayyih, Mohammed K. Khashan, Nawfel M. Baqer and Muna S. Kassim (2025) 'Enhancement of heat transfer numerically by inserting helical coiled wire inside tube flow', Kufa Journal of Engineering, 16(4), 179-190.

Maher A.R. Sadiq Al-Baghdadi (2020) 'Experimental and CFD study on the dynamic thermal management in smartphone and using graphene nano sheets coating as an effective cooling technique', International Journal of Energy and Environment (IJEE), 11(2), 97-106.

Manno, M., Yang, B., Khanna, S., McCluskey, P. and Bar-Cohen, A. (2015) 'Microcontact-enhanced thermoelectric cooling of ultrahigh heat flux hotspots', IEEE Transactions on Components, Packaging and Manufacturing Technology, 5(12), 1775-1783.

Moffat, R.J. (1985) 'Using uncertainty analysis in the planning of an experiment', Journal of Fluids Engineering, 107(2), 173-178.

Murtadha A. Hanoon, Mohsen H. Farj. and Kameel, S.Mekki (2025) 'Enhancement of heat transfer numerically by inserting helical coiled wire inside tube flow', Kufa Journal of Engineering, 16(3), 1-21.

Ning Li, Yibo Zhang, Yawei Xu, Jing Li. (2025) Graphene/epoxy coating with radiation heat dissipation properties for spacecraft thermal management, Chemical Engineering Journal, 519(September).

Premkumar M., Santhanakrishnan R., Arulprakasajothi M. and Suresh V. (2024) Heat Dissipation Effects of Different Nano coated Lateral Fins An Experimental Investigation. THERMAL SCIENCE. 28(1A), pp. 293-305.

Raad H. Abed. and Nabeel A. Ghyadh (2024) 'INVESTIGATION OF HYBRID PHOTOVOLTAIC /THERMAL SOLAR SYSTEM PERFORMANCE UNDER IRAQ'S CLIMATE CONDITIONS', Kufa Journal of Engineering, 15(1), 1-18.

Sabatino, D. and Yoder, K. (2014) 'Pyrolytic graphite heat sinks: A study of circuit board applications', IEEE Transactions on Components, Packaging and Manufacturing Technology, 4(6), 999-1009.

Sahin, B. and Demir, A. (2008) 'Thermal performance analysis and optimum design parameters of heat exchanger having perforated pin fins', Energy conversion and management, 49(6), 1684-1695.

Şara, O.N. (2003) 'Performance analysis of rectangular ducts with staggered square pin fins', Energy Conversion and Management, 44(11), 1787-1803.

Sarvar, F., Whalley, D.C. and Conway, P.P., 2006, September. Thermal interface materials-A review of the state of the art. In (2006) 1st electronic systemintegration technology conference (Vol. 2, pp. 1292-1302) IEEE.

Shahil, K.M. and Balandin, A.A. (2012) 'Thermal properties of graphene and multilayer graphene: Applications in thermal interface materials', Solid state communications, 152(15), 1331-1340.

Tsai, W.Y., Huang, G.R., Wang, K.K., Chen, C.F. and Huang, J.C. (2017) 'High thermal dissipation of Al heat sink when inserting ceramic powders by ultrasonic mechanical coating and armoring', Materials, 10(5), 454.